4th AIAA Atmospheric and Space Environments Conference
25 - 28 June 2012, New Orleans, Louisiana

AIAA 2012-3132

# SLD Lagrangian modeling and capability assessment in the frame of ONERA 3D icing suite

Ph. Villedieu[1], P. Trontin[2], D. Guffond[3], D. Bobo[4]
*ONERA - The French Aerospace Lab - F-31055, Toulouse, FRANCE*

**On the basis of an existing model for spray wall interactions, a SLD model has been implemented in the Lagrangian solver of the 3D icing suite developed by ONERA. This new model has been validated against some test cases issued from the NASA SLD experimental database. The aim of this paper is to present the current status of this on-going research activity.**



## Nomenclature

d : Droplet Diameter (m)
t : Time (s)
$\tau_{bup}$ : Droplet break-up time (s)
$\tau_p$ : Droplet dynamical response time (s)
r : Droplet radius (m)
m : Mass (kg)
$h_R$ : Roughness height (m)
$h_f$ : Liquid film thickness (m)
**v** : Velocity ($m.s^{-1}$)
**u** : Velocity ($m.s^{-1}$)
**g** : Gravity acceleration ($m.s^{-2}$)
**x** : Space coordinates or droplet position (m)
$\mathbf{n}_W$ : Normal to the wall unit vector
**n** : Normal unit vector
ρ : Density (kg.m-3)
μ : Dynamic Viscosity ($kg.m^{-1}.s^{-1}$)
σ : Surface Tension (kg.s-2)
$\theta_0$ : Incidence angle (°)
$C_D$ : Droplet drag coefficient
We : Weber Number based on the normal to the wall velocity component
Re : Reynolds Number
Oh : Ohnesorge Number
K : Cossali Number = We $Oh^{-2/5}$
δ = Dimensionless film thickness = $h_f/d_0$
R : Dimensionless roughness height = $h_R/d_0$

**Subscripts**
*l:* Liquid (water)
*g:* Gas (air)
*d*: Droplet
*p*: Particle or Droplet
*i*: Numerical particle
*0*: Before wall impact or break-up
*1, s*: After splashing or break-up
*1, b*: After bouncing
*n* : Normal component or time step number
*t* : Tangential component

[1] Senior scientist, Aerodynamics and Energetic modelling department, philippe.villedieu@onera.fr
[2] Research engineer, Aerodynamics and Energetic modelling department, pierre.trontin@onera.fr
[3] Icing expert, Aerodynamics and Energetic modelling department, didier.gufond@onera.fr
[4] Internship engineer student, Aerodynamics and Energetic modelling department, david.bobo@onera.fr

# I. Introduction

Icing occurs when an aircraft flies through clouds in which super cooled droplets are suspended, with an ambient air temperature below the freezing point. The droplets impinge on the aircraft surfaces and freeze, leading to ice accretion. The resulting change in the aircraft geometry can modify aerodynamic characteristics (loss of lift, rise of drag), can affect the ability of the probes to provide accurate measurements, can clog air intake or even damage the engine by ice ingestion, and in the worst scenario can cause a complete loss of the control of the aircraft. Airframe icing is therefore a topic of great interest for the aerospace industry and, more particularly, for airframers, because it deals with the safety and efficient operation of aircrafts under all weather conditions.

The importance of proper ice control for aircraft operation in cold climates was recently highlighted by several in flight icing events and crashes. In 1994, an ATR-72 crashed at Roselawn, Indiana, USA. It has been speculated that this accident was due to Super-cooled Large Droplet (SLD). This crash leads to a modification of the regulation rules with the definition of the Appendix O which includes freezing drizzle and freezing rain icing conditions. The associated NPRM (Notice for Proposed Rule Making) has been distributed to industry for comments on 29th June 2010 and could be applicable by beginning 2012. In order to comply with this new rule, the simulation tools, as Means of Compliance, have to be improved and validated for these conditions.

This paper presents activities performed in the frame of a collaboration between ONERA and AIRBUS on SLD icing phenomena in order to implement an SLD (Lagrangian) model in ONERA 3D icing suite (ONICE3D) and to evaluate its capability to reproduce experimental results from the SLD NASA database, with the aim to be able to further assess the potential impact at A/C level. A similar work has been done previously[1] in the case of ONICE2D, the ONERA 2D icing suite. The main differences lie in the 3D framework and in the SLD model itself which here has been derived from an existing model[2] developed for droplet impingement in the context of combustion chamber applications.

The paper is organised as follow. Part 2 is devoted to a short presentation of ONICE3D, the ONERA 3D icing suite with a focus on the Lagrangian trajectory module. Part 3 addresses the SLD model. After having recalled the main physical phenomena, we present ONERA SLD model and compare it to other existing models issued from the literature[3-4]. Part 4 is concerned with the model assessment. Selected test cases from the NASA SLD database[5] have been considered and ONICE3D results have been compared with experimental results as well as ONICE2D and LEWICE2D numerical ones. Lastly part 5 is devoted to conclusion and way forward.

# II. Description of ONERA 3D icing suite

## A. ONICE3D architecture

A recognized general methodology used for the simulation of ice accretion is based on the successive computation of air flow, water droplet trajectories, collection efficiency, heat transfer balance and accreted ice. Figure 1 presents the general flow chart of the ice accretion process.

The flow field and associated convective heat transfer are computed using an inviscid approach (Panel method, potential method, Euler method, etc.) coupled with boundary layer calculation or a viscid approach (RANS). The balance of forces acting on the droplets determines their trajectories and the collection efficiency coefficient. Using these inputs, the resolution of the thermal and mass balance makes it possible to determine the ice thickness and then the ice shape on the considered surfaces.

ONICE3D is a comprehensive modular ice accretion suite developed by ONERA for 3D icing problems. Unlike ONICE2D, each module of ONICE3D can be used in a stand-alone mode and / or can be replaced by another external module. This more general architecture has been required by industrial partners of ONERA to enable easy and secured implementation of ONERA icing suite in their own CFD environment. The interoperability between all modules is ensured through a CGNS neutral layer with a restriction to the CGNS standard for icing purpose. Under this constraint, an in-house solver can be substituted to any of the specific components of the suite. Most modules of ONICE3D (Navier-Stokes solver, Particle Trajectory solvers) are themselves part of CEDRE[6a] suite, which is a multi-physics CFD platform developed by ONERA for general applications in the Energetic field[6b].

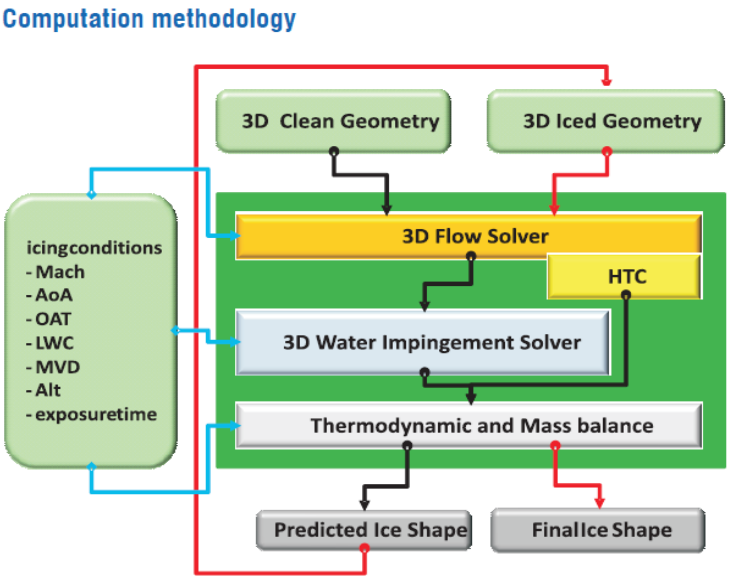


***Fig. 1 :*** *Flow chart describing the predictor/corrector method to obtain a final ice shape*

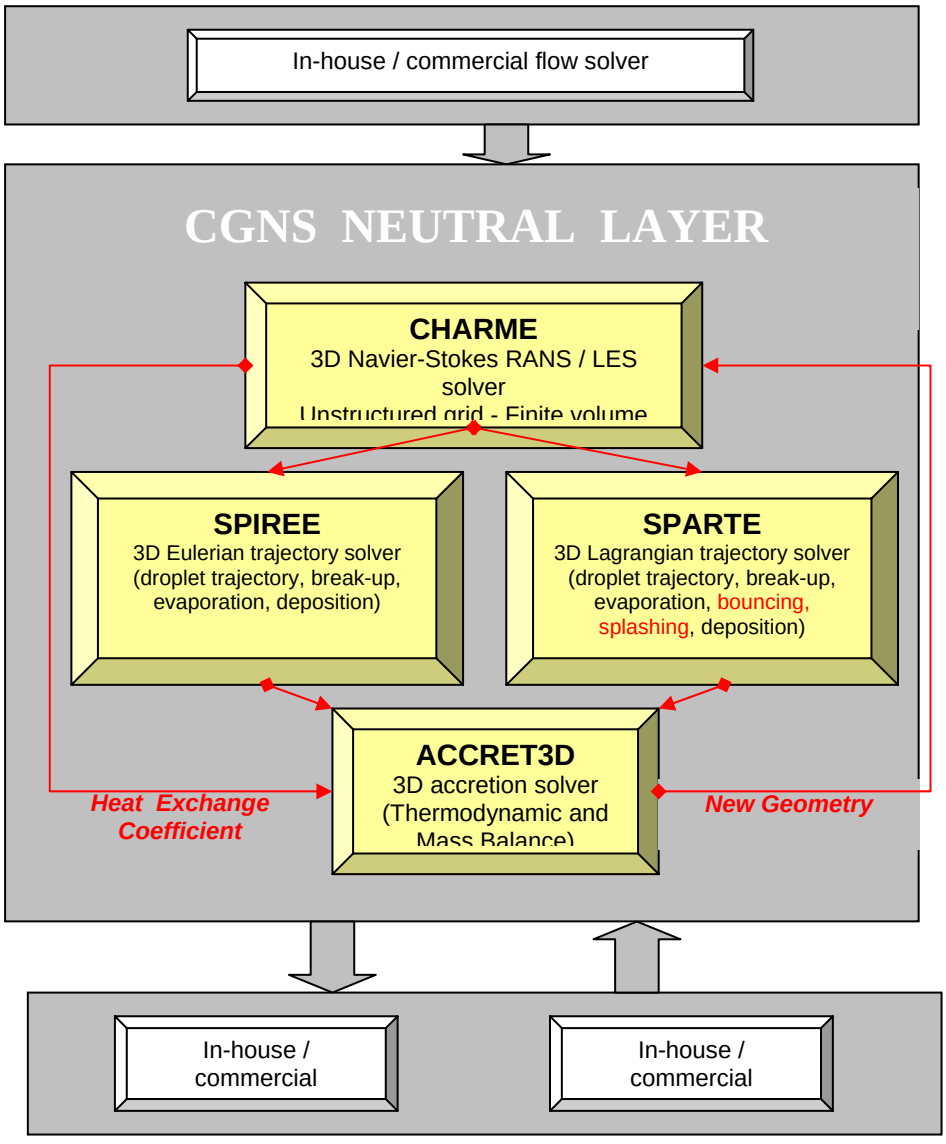


**Fig. 2 :** *Flow chart describing the ONICE3D architecture and interactions with other external solvers.*

As sketched in Fig. 2, ONICE3D icing suite is presently composed of 4 solvers: CHARME (RANS / LES Navier-Stokes solver) which can be used for the gas flow field and the heat exchange coefficient computation, SPIREE (Eulerian dispersed phase solver) and SPARTE (Lagrangian dispersed phase solver) which can be used for computing the droplet collection efficiency and ACCRET3D which is a Messinger's approach based ice accretion module.

Until now the SLD capability (e.g. the capability of dealing with rebound and splashing phenomena) has only been implemented in the Lagrangian trajectory solver. Extension to the Eulerian solver SPIREE is scheduled for the forthcoming years. We refer to [7] for a detailed description of SPIREE models and numerical methods. In the next subsection, we focus on SPARTE which is the only solver of ONICE3D which has been used in the present study.

### B. Focus on ONICE3D Lagrangian trajectory solver

The SPARTE solver is devoted to the simulation of a dispersed phase (composed of solid particles or droplets) suspended in a gas flow. It is based on a Lagrangian approach which means that the particulate phase is simulated by computing the evolution of a large number of numerical particles (parcels) equipped with variables of position, velocity, size and temperature, or other relevant quantities. The mean dispersed phase properties are obtained by averaging over a representative sample of parcels that cross a defined volume, within a certain time interval. The particulate phase can be composed of particles of different physical states (solid or liquid) and compositions. Specific models (drag coefficient, heat exchange, fusion/solidification, evaporation/condensation, collision/coalescence …) may be chosen independently for each type of particle. As regards the boundary conditions, the following are currently available: walls with various interaction models, inlet with particle emission, outlet (free boundary), spatial periodicity, mixing plane (for a surface separating a rotating domain from a fixed one). Here, we present the only features which are involved for SLD icing applications, e.g. drag force model, break-up model and impingement model. For a more detailed description of SPARTE module we refer to [7].

For icing applications, the volume fraction of the particulate phase (droplets, ice-crystals, mixed phase particles) is assumed to be small enough for the particle influence on the gas flow to be negligible. Hence a sequential one-way-coupling procedure is applied which consists of computing first the stationary mean gas flow field and then to compute a statistically representative set of particle trajectories, assuming that the mean gas flow field is frozen and not influenced by the presence of the particles. In practice, droplet trajectories are emitted from the inlet boundary of the computational domain (from a limited zone) and calculated independently from each other until they reach a solid surface or leave the computational domain. A given mass flow rate (depending on the far field conditions: Liquid Water Content, Mach number, cloud droplet size distribution) is affected to each emitted trajectory. Therefore, summing on all trajectories, it is possible to compute the deposited mass flow rate on any face of the solid surface mesh (for the collection efficiency computation) or the local liquid water content in any cell of the mesh (by taking into account the residence time of each trajectory in the considered cell).

In order to reduce the computational time, a local time step procedure has been implemented in SPARTE. At each iteration and for each numerical particle, the value of the time step is based on the estimated residence time of the particle in the cell in which it is located. Typically, the expression of the time step writes:

$$\Delta t_i^n = \gamma \frac{\delta(C_i^n)}{\left\| \mathbf{v}_i^n \right\|}, \quad \text{with} \quad \delta(C_i^n) = vol(C_i^n)^{1/3}, \tag{1}$$

where $\gamma$ is a user-defined adjustable parameter (in practice $\gamma = 0.2$ leads to a good compromise between cost and trajectory accuracy), $C_i^n$ is the cell where particle $i$ is located at the beginning of time iteration $n$ and $\mathbf{v}_i^n$ is the particle velocity. Each time iteration is divided in two steps: *a fragmentation step* during which droplet break-up phenomena are taken into account and *a transport step* during which motion equations are integrated and particles are moved to their new position. Boundary conditions, including droplet impingement onto a solid surface, are accounted for during the transport step. This aspect will be detailed in the next section of the paper.

**Transport step.** The droplet motion equation which is used in SPARTE for icing applications writes:

$$(2)\qquad \begin{cases} \dfrac{d\mathbf{x}_d}{dt} = \mathbf{v}_d \\ m_d \dfrac{d\mathbf{v}_d}{dt} = \dfrac{1}{2}\rho_g C_D \pi r_d^{\,2} \left\| \mathbf{u}_g(\mathbf{x}_d) - \mathbf{v}_d \right\| \left( \mathbf{u}_g(\mathbf{x}_d) - \mathbf{v}_d \right) + m_d \mathbf{g} \end{cases}$$

where $\mathbf{x}_d$ denotes the droplet position, $\mathbf{v}_d$ the droplet velocity, $m_d = \dfrac{4}{3}\rho_l \pi r_d^{\,3}$ the droplet mass, $r_d$ the droplet radius, $\mathbf{u}_g(t,\mathbf{x}_d)$ the gas (air) velocity at the droplet location and $C_D$ the droplet drag coefficient given by Schiller and Naumann correlation:

$$(3)\qquad C_D = \frac{24}{\mathrm{Re}_d}\left(1 + 0.15\,\mathrm{Re}_d^{0.687}\right) \quad \text{with} \quad \mathrm{Re}_d = \frac{2\rho_g r_d \left\| \mathrm{v_d} - \mathrm{u_g} \right\|}{\mu_g} < 800$$

Several numerical schemes can be used to integrate Eq. (2) according to the desired compromise between cost, accuracy and numerical stability constraint. In SPARTE, the following scheme is used:

$$(4)\qquad \begin{cases} \mathbf{x_i^{n+1}} = \mathbf{x_i^n} + \mathbf{u}_g(\mathbf{x_i^n})\Delta t + \left[ \mathbf{v_i^n} - \mathbf{u}_g(\mathbf{x_i^n}) \right] \left[ 1 - \exp(-\dfrac{\Delta t}{\tau_p^n}) \right] \tau_p^n + \left[ \Delta t - \left( 1 - \exp(-\dfrac{\Delta t}{\tau_p^n}) \right) \tau_p^n \right] \tau_p^n \mathbf{g} \\ \mathbf{v_i^{n+1}} = \mathbf{u}_g(\mathbf{x_i^n}) + \exp(-\dfrac{\Delta t}{\tau_p^n}) \left[ \mathbf{v_i^n} - \mathbf{u}_g(\mathbf{x_i^n}) \right] + \left[ 1 - \exp(-\dfrac{\Delta t}{\tau_p^n}) \right] \tau_p^n \mathbf{g} \end{cases}$$

where $\tau_p = \dfrac{24}{\mathrm{Re}_d\, C_D}\left( \dfrac{2\rho_l r_d^2}{9\mu_g} \right)$ denotes the droplet dynamical response time ($\rho_l$ being the liquid density and $\mu_g$ the gas dynamical viscosity). Equation (4) is an unconditionally stable first order scheme, which corresponds to the exact solution of Eq. (2) for constant gas velocity field and very small Reynolds number (Stokes drag law). Higher order explicit schemes (like Runge-Kuta schemes) can also be used but they are only conditionally stable and their stability condition is very constraining for small particles (because $\tau_p \rightarrow 0$).

**Fragmentation step.** A Monte-Carlo algorithm is used during this stage to avoid the creation of too many new numerical particles. The algorithm used in SPARTE reads as follows:

i) For each numerical particle present in the computational domain, compute the Weber number defined as:

$$We_i^n = \frac{2\rho_g(\mathbf{x}_i^n) \left\| \mathbf{v_i^n} - \mathbf{u}_g(\mathbf{x}_i^n) \right\|^2 r_i^n}{\sigma},$$

with $\rho_g$ being the gas density and $\sigma$ the surface tension coefficient.

ii) If $We_i^n > We^*$ (where $We^* = 12$ denotes the threshold Weber number for droplet break-up) then compute the particle break-up probability during the current time step : $\pi_i = 1 - \exp(-\dfrac{\Delta t}{\tau_i^{bup}})$, where $\tau_i^{bup}$ denotes the mean break-up duration, given by the following empirical correlation [8a,b]:

$$\tau_i^{bup} = 5\sqrt{\frac{\rho_l}{\rho_g}}\,\frac{2r_i^n}{\left\| \mathbf{v}_i^n - \mathbf{u}_g(\mathbf{x}_i^n) \right\|}.$$

iii) Choose a random number $\alpha$ uniformly distributed between 0 and 1; if $\alpha < \pi_i$ then fragmentation of the $i^{th}$ particle is considered to occur during the current time step and new numerical particles are created; the radius of each new particle is then randomly chosen according to the model used for the n.d.f. (number density function) $h^{bup}$ of the resulting droplets; the number of "children" numerical particles is usually chosen between 1 and 5 to ensure a good compromise between accuracy and computational cost.

The number size distribution of the droplets issued from the break-up of a given droplet of radius $r_0$ is assumed to follow an exponential law like in the model proposed by Amsden [9]:

(5) $$h_{bup}(r,r_0)=\frac{r_0^3}{6r_*^4}\exp\left(-\frac{r}{r_*}\right),$$

where $r_0$ is the initial droplet radius, $r_*$ is a positive parameter depending on $r_0$, which has to be fitted thanks to some experimental data. It is worth noticing that $r_*$ can be easily expressed as a function of the Sauter mean radius $r_{32}^{bup}$ of the secondary droplets:

(6) $$r_{32}^{bup}\overset{def}{=}\frac{1}{3}\left[\int_{\mathbf{R}^+} r^3 h_{bup}(r,r_0)dr\right]\left[\int_{\mathbf{R}^+} r^2 h_{bup}(r,r_0)dr\right]^{-1}=3\,r_*,$$

which, itself, can be calculated according to Wert [10] empirical correlation:

(7) $$\frac{r_{32}^{bup}}{r_0}=\begin{cases}0.32\ We^{-1/3}\left(\dfrac{4.1}{(We-12)^{1/4}}\right)^{2/3}, & if \quad We\in[12,18[\\ 0.32\ We^{-1/3}\left(\dfrac{2.45(We-12)^{1/2}-1.9}{(We-12)^{1/4}}\right)^{2/3}, & if \quad We\in[18,45[\\ 0.32\ We^{-1/3}\left(\dfrac{12.2}{(We-12)^{1/4}}\right)^{2/3}, & if \quad We\in[45,+\infty[\end{cases}$$

Finally, the fragment velocities are given by the following correlation issued from [8a,b]:

(8) $$\mathbf{v}^{bup}(r,r_0)=\mathbf{u}_g(\mathbf{x}_d)-\frac{\mathbf{u}_g(\mathbf{x}_d)-\mathbf{v}_0}{1+2.7\left(\sqrt{\dfrac{\rho_g}{\rho_l}}\dfrac{r}{r_0}\right)},$$

where $\mathbf{v}_0$ denotes the droplet velocity before break-up.

In NASA-LEWICE model [4-5], droplets start to break if We > 13, which is very close to the threshold value used in the SPARTE model (We* = 12), but for simplicity sake all secondary particles are supposed to have the same size $r_s$, given by the following expression:

(9) $$\frac{r_s}{r_0}=6.2\left(\frac{\rho_g}{\rho_l}\right)^{-1/4}\left(\frac{2\rho_l\left\|\mathbf{v}_g-\mathbf{v}_d\right\|r_0}{\mu_l}\right)^{-1/2},$$

which can also be written as:

(10) $$\frac{r_s}{r_0}=6.2\left(\frac{2r_0\rho_g\left\|\mathbf{v}_d-\mathbf{v}_g\right\|^2}{\sigma}\right)^{-1/4}\left(\frac{\mu_l^{\,2}}{2r_0\rho_l\sigma}\right)^{1/4}=6.2\ \sqrt{Oh}\ We^{-1/4},$$

which is very different from Wert correlation[10] which is used in SPARTE. A comparison between LEWICE and SPARTE model is shown in Fig. 3. We observe that the agreement is better than expected, especially for $d_0 = 2\ r_0 = 200\ \mu m$.

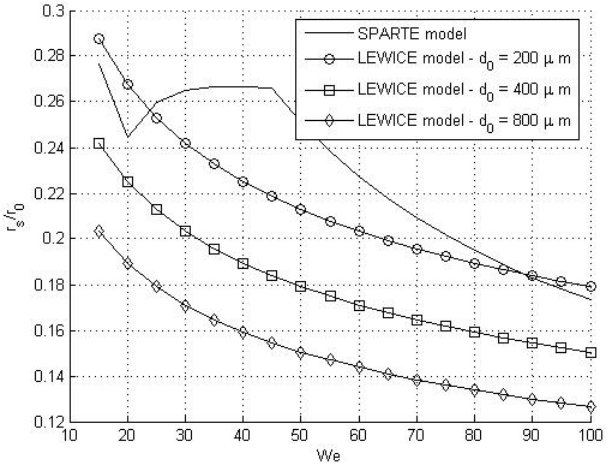


***Fig. 3 :*** *Comparison between SPARTE and LEWICE break-up model for $r_s/r_0$*

## III. Droplet impingement model

### A. Description of main physical phenomena

Number of complex physical phenomena can occur when droplets impinge a solid surface. Droplet properties (size, velocity …), liquid properties (viscosity, surface tension, density …), surface properties (temperature, roughness, presence or not of a liquid film …) and gas properties (density, viscosity …) can play a role on the result of the impingement.

If the surface temperature is lower than the liquid ebullition temperature (which is of course the case for icing applications), four kinds of interaction can be experimentally observed, mainly depending on the normal to the wall velocity component of the impinging droplet:

- ***Droplet sticking:*** when the normal impact velocity is very low, the droplet adheres to the wall.
- ***Droplet bouncing***: when increasing the normal impact velocity, lubrication forces due to the thin air film trapped between the droplet and the wall prevent the droplet to touch the solid surface and the droplet bounces off the wall (Fig. 4).
- ***Droplet deposition/spreading:*** when increasing again the normal impact velocity, the droplet spreads on the wall, to form a wall film or to merge with the existing water film; the droplet initial kinetic energy is partly dissipated by viscosity forces and partly transformed into surface tension energy (Fig. 4).
- ***Droplet splashing:*** finally, when increasing again the normal impact velocity, viscous forces can no longer dissipate the kinetic energy and surface tension fails to maintain droplet cohesion. The droplet splashes into smaller ones and some of them are ejected from the wall. The total ejected mass is inferior to the initial droplet mass and increases as the impact velocity increases (Fig. 4).

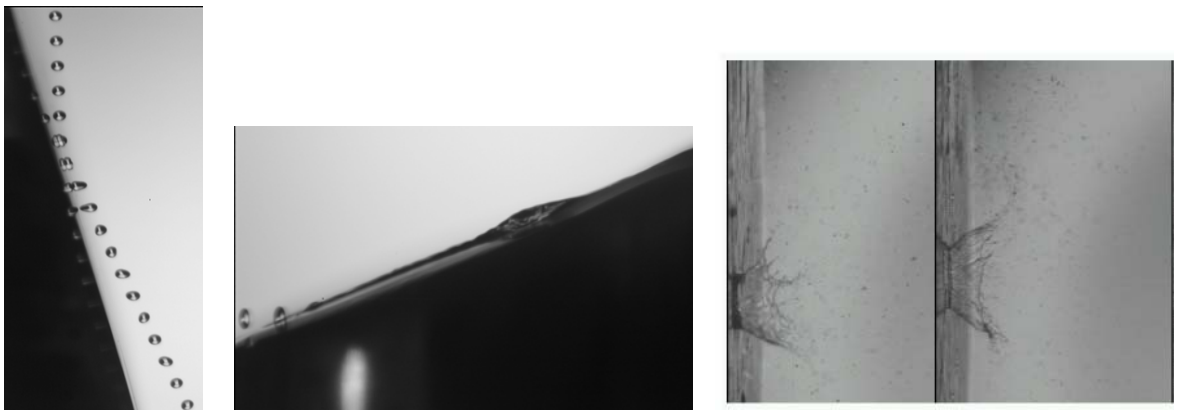

***Fig. 4:*** *Droplet impingement regimes. Left: bouncing. Centre: deposition with film formation. Right: splashing for two different velocities*

## B. SPARTE impingement model

SPARTE impingement model has been first designed for spray combustion applications [2] involving hot wall temperature and Leidenfrost effects and has been adapted for SLD icing applications in the frame of the present study.

### B.1. Impingement regime thresholds

The droplet sticking regime (which correspond to very low normal impact velocity) is not taken into account because of its very low occurrence probability. For a wall surface whose temperature is lower than the liquid ebullition temperature, the thresholds between the different impingement regimes are computed according to the following model:

$$\begin{array}{ll} K < K_{b0}\ f_b(R,\delta) & \rightarrow \text{bouncing regime} \\ K_{b0}\ f_b(R,\delta) < K < K_{s0}\ f_s(R,\delta) & \rightarrow \text{spreading / deposition regime,} \\ K > K_{s0}\ f_s(R,\delta) & \rightarrow \text{splashing regime} \end{array} \quad (11)$$

where $K$ denotes the Cossali number. $K$ is defined as: $K = We \times Oh^{-2/5}$, where $We$ is the Weber number and $Oh$ is the Ohnesorge number defined as:

$$We = \frac{2\rho_l r_0 (\mathbf{v}_0.\mathbf{n}_w)^2}{\sigma} \quad , \qquad Oh = \sqrt{\frac{\mu_l}{2\rho_l \sigma r_0}} \quad ,$$

with $\mathbf{n}_w$ the unit normal to the wall surface, $r_0$ the droplet radius and $\mathbf{v}_0$ he droplet velocity, before the impact. $K_{s0}$ and $K_{b0}$ are threshold values corresponding to a very smooth (R=0) solid surface and $f_s$, $f_b$ are correction coefficients which allow to account for the influence of wall roughness and liquid film thickness on the bouncing and splashing thresholds. The dimensionless wall roughness height and film thickness are defined as $R = \frac{h_r}{2r_0}$, $\delta = \frac{h_f}{2r_0}$ where $h_r$ denotes the average roughness height and $h_f$ the film thickness. The currently implemented models for the correction factors $f_b$ and $f_s$, write:

$$f_s(R,\delta) = \frac{1+\tilde{R}^2}{1+\omega_{sr}\tilde{R}^2}\frac{1+\delta^2}{1+\omega_{sf}\delta^2} \quad \text{and} \quad f_b(R,\delta) = \frac{(1+\tilde{R}^2)}{(1+\omega_{sr}\tilde{R}^2)(1+\omega_{br}\tilde{R}^4)}\frac{1+\delta^2}{1+\omega_{bf}\delta^2} \quad , \quad (12)$$

where $\tilde{R} = \frac{R^2}{R+\delta}$ is a modified wall roughness due to the presence of the liquid film and where $\omega_{sr}$ , $\omega_{sf}$, $\omega_{br}$ and $\omega_{bf}$ are adjustable empirical constants. These bouncing and splashing models both exhibit asymptotic behaviours:

- for large values of the dimensionless roughness ($\delta = 0, R \rightarrow +\infty$): in that case, for the splashing threshold one has: $K^*_s \rightarrow K_{s1} = K_{s0}/\omega_{sr}$, whereas for the bouncing threshold one has: $K^*_b \rightarrow K_{b1} = 0$ (rebound is not possible on a too rough surface). The value of $\omega_{sr}$ and $\omega_{br}$ will be precised bellow.
- for large values of the dimensionless film thickness (R fixed, $\delta \rightarrow +\infty$ ): in that case, for the splashing threshold one has: $K^*_s \rightarrow K_{s2} = K_{s0}/\omega_{sf}$, whereas for the bouncing threshold one has: $K^*_b \rightarrow K_{b2} = K_{b0}/\omega_{bf}$. The value of $\omega_s$ and $\omega_b$ will be précised bellow.

The following table summarizes parameter values which have been used in the frame of the present study.

| $K_{s0}$ | $K_{b0}$ | $\omega_{sr}$ | $\omega_{sf}$ | $\omega_{br}$ | $\omega_{bf}$ |
|---|---|---|---|---|---|
| 3000 | 600 | 20/3 | 5/6 | 32 | 1 |

***Tab. 1:*** *Summary of the impingement model parameters*

$\omega_{sr} > 1$ accounts for the experimental fact that splashing is more likely to occur on a rough wall than on a smooth one. Conversely $\omega_{sf} < 1$ accounts for the experimental fact that deposition is less likely to occur on a smooth dry wall than on a liquid pool. The value $\omega_{bf} = 1$ only means that, for smooth wall, the influence of the liquid film thickness is presently not taken into account on the bouncing/deposition threshold.

### B.2. Impingement mass loss

A very important feature of the model for icing application is the expression of the splashing and bouncing mass losses. In SPARTE, the initial model wrote:

$$\frac{m_s}{m_0} = 1 - \left( \frac{K_s^*}{K} \right)^{1/2} , \qquad \frac{m_b}{m_0} = 1 \quad , \tag{13}$$

where $m_s$ is the mass of the splashing droplets, $m_b$ is the mass of the bouncing droplet and $K_s^* = f_s(R,\delta) K_{s0}$ denotes the splashing / deposition threshold.

For large values of K, this model yields a very high mass loss and does not fit at all with the experimental results from [5].To get a better agreement, the following model has been retained:

$$\frac{m_s}{m_0} = \max\left( a(\theta_0) - \left( \frac{K_s^*}{K} \right)^{b(\theta_0)} , 0 \right) \quad , \qquad \frac{m_b}{m_0} = 1 \quad , \tag{14}$$

where $\theta_0$ is the incidence angle (angle between the wall and the incident velocity). By construction of the model, $a(\theta_0)$ corresponds to the asymptotic mass loss for high normal velocity impact ($K \rightarrow +\infty$ ). To be able to account for the experimental results obtained by NASA[5], the splashing mass loss must be a decreasing function of the incidence angle, like in the refined NASA LEWICE model[4]. The highest the incidence angle, the smallest the mass loss due to reemitted splashing droplets. After several guesses, The following expressions have been retained in SPARTE for $a(\theta_0)$ and $b(\theta_0)$:

$$a(\theta_0) = 1 - 0.3\sin(\theta_0) , \qquad b(\theta_0) = \frac{1}{8} \left[ 1 + 3\cos(\theta_0) \right] . \tag{15}$$

According to these formula, it is worth noticing that the maximum value of the mass loss, $a(\theta_0)$, is assumed to lie between 0.7 for high incidence angle ($\theta_0$ close to 90°) and 1 for low incidence angle ($\theta_0$ close to 0°). Similarly the exponent $b(\theta_0)$ is assumed to lie between 1/8 and 1/2.

### B.3. Post splashing droplet size and velocity distributions

The model used for calculating the splashed droplet velocity distribution has been first described in [2]. It is inspired from the model derived by Schmell, Rosskamp,Willmann and Wittig [11] and the works of Mundo, Sommerfeld and Tropea [12]. In this approach, impinging droplet velocity $\mathbf{v}_0$ is decomposed into two components, one perpendicular to the solid wall, and the other, parallel to the solid surface, respectively denoted $\mathbf{v}_{n,0}$ and $\mathbf{v}_{t,0}$. The phenomenon is then separated into two kinds of contributions: normal splashing and tangential splashing. Tangential splashing only originates a nonzero tangential splashed velocity $\mathbf{v}'_{t,1}$ whereas normal splashing originates a splashed velocity $\mathbf{v}''_1$, which is neither normal nor tangential. The final splashed velocity is obtained by adding the two contributions, giving $\mathbf{v}_1 = \mathbf{v}'_{t,1} + \mathbf{v}''_1$. The following Weibull probability law determines the magnitude of vector $\mathbf{v}''_1$ :

$$P(x) = \frac{2.5}{0.35} \left[ \frac{x}{0.35} \right]^{1.5} \exp\left[ - \left[ \frac{x}{0.35} \right]^{2.5} \right], \quad \text{with} \quad x = \frac{\left\| \mathbf{v}''_1 \right\|}{\left\| \mathbf{v}_{n,0} \right\|} . \tag{16}$$

Then, the orientation of vector $\mathbf{v}''_1$ is defined by its elevation $\alpha$ and azimuth $\beta$, which are determined using a uniform probability law, in the ranges of 0° to 25° for $\alpha$ and 0° to 360° for $\beta$. Having angle $\beta$ take any possible value from an arbitrarily-set reference axis, agrees with the fact that a normal impact originates a symmetrical cloud of splashed drops. Tangential splashing will be regarded as a constant tangent velocity damp, which leads to:

$$\mathbf{v}'_{t,1} = 0.8\ \mathbf{v}_{t,0} . \tag{17}$$

As regards the droplet size probability density function, it is assumed that whatever the value of K (supposed to be greater than the splashing threshold), the splashing impact of a single droplet creates a cloud of smaller droplets with a lognormal size distribution defined as:

$$P(r) = \frac{1}{\sqrt{2\pi\upsilon}\cdot r}\exp\left[-\frac{1}{2\upsilon}\left(\ln\frac{r}{r_m}\right)^2\right]. \tag{18}$$

It is defined by the two following parameters, mean diameter $d_m$ and variance $\upsilon$. A Fitting of experimental data from [11] and [13] leads to the following correlation

$$\frac{r_m}{r_0} = A_0 + A_1\exp\left(\frac{-K}{\Delta K}\right), \tag{19}$$

where $A_0 = 0.09$, $A_1 = 0.51$ and $\Delta K = 1500$. Regarding distribution variance, although a simple correlation could not be derived, the following constant is proposed, as found in several experimental histograms from [11]: $\upsilon = 0.2$.

### B.4. Post bouncing droplet velocity

The model used for calculating the post impact velocity reads as follows:

$$\begin{cases} \mathbf{v}_{n,1} = 4\mathbf{v}_{n,0}\left[\sqrt{\dfrac{K}{K_b^*}} - \dfrac{K}{K_b^*}\right] \\ \mathbf{v}_{t,1} = 0.8\ \mathbf{v}_{t,0} \end{cases} \quad \text{with} \quad K_b^* = f_b(R,\delta)K_{b0}, \tag{20}$$

where $\mathbf{v}_{n,1}$ and $\mathbf{v}_{t,1}$ respectively denote the normal and tangential post-impact velocity. Note that according to Eq. (20), the maximum value of the restitution coefficient $v_{n1}/v_{n0}$ is reached for $K/K_b^* = 0.5$ and is equal to 0.83. For $K \rightarrow 0$ (sticking regime), one has $v_{n1}/v_{n0} \rightarrow 0$ and for $K \rightarrow K_b^*$ (deposition regime) one also has $v_{n1}/v_{n0} \rightarrow 0$.

## IV. Model assessment

A comparison of ONICE3D results with NASA SLD experimental results has been carried out. Only 4 test cases of the 114 test cases that count the NASA SLD database were considered. The comparison presented hereafter refers to the experiments performed by Papadakis et al[5]. They performed different measurements (pressure distribution, collection efficiency coefficient β) on a NACA23012 airfoil with or without ice shape for a Mach number 0.2, an angle of attack of 2.5° and with different MVDs. Both 10-bin and 27-bin droplet distributions are provided. Figure 5 presents a view of the NACA23012 airfoil installed in the NASA Glenn Icing Research Tunnel.

Figures 6-8 present a comparison of the β coefficient obtained with ONICE3D ONICE2D and LEWICE and in experiment on the clean NACA23012 airfoil for three MVDs: 52μm, 154μm and 236μm. All ONICE3D calculations have been performed with the 10-bin droplet distribution. ONICE3D results correspond to the blue and orange curves. The blue curve has been obtained without activating the SLD whereas the orange curve has been obtained with the above described model. Figure 9 presents a comparison of the β coefficient obtained with ONICE2D, LEWICE and in experiment for a 111μm MVD on the NACA23012 airfoil with 10min ice shape. For all test cases, it has been assumed that the mean surface roughness height (blotter strip) was equal to: $h_R = 20$ μm and that there was no liquid film on the impacted surface: $h_f = 0$.

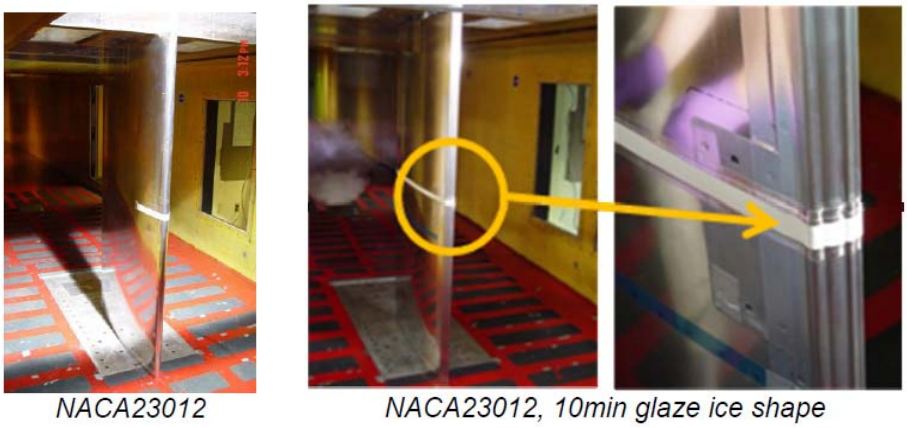


***Fig. 5:*** *NACA23012 airfoil installed in the NASA Glenn IRT.*

Figures 6-8 show that the activation of the SLD model allows a much better agreement between ONICE3D results and the NASA icing tunnel measurements over the full range of MVD from 52µm to 236µm. Compared to LEWICE and ONICE2D (with almost the same model as LEWICE, see [1]), ONICE3D SLD model provides slightly better results on the lower side of the airfoil but tends to overestimate the collection efficiency on the upper side. Figure 8 shows that the activation of ONICE3D break-up model slightly improves the agreement with NASA experimental data but is of second order importance in the present case.

As shown in Fig. 10, droplet break-up can not occur if the droplet diameter is lower than a given critical value (depending on the geometry and the Mach number) either because the threshold Weber number ($We^* \approx 12$) is not reached or because the duration of the break-up is too long for being finished before droplet impingement. On the other hand, when break-up occurs, droplets produced by the fragmentation process have a smaller dynamical response time than the initial droplet and are swept by the aerodynamic flow around the airfoil (see Fig. 10).

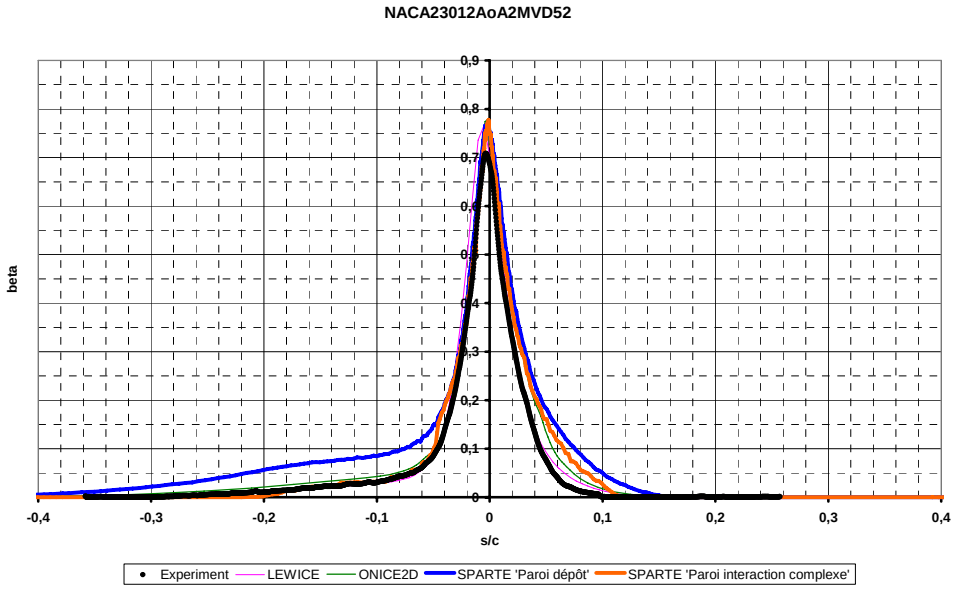


***Fig. 6: NACA23012 - Collection efficiency, MVD = 52 µm***
*Black line: experiment - Blue line: ONICE3D without SLD model - Orange line: ONICE3D with SLD model*

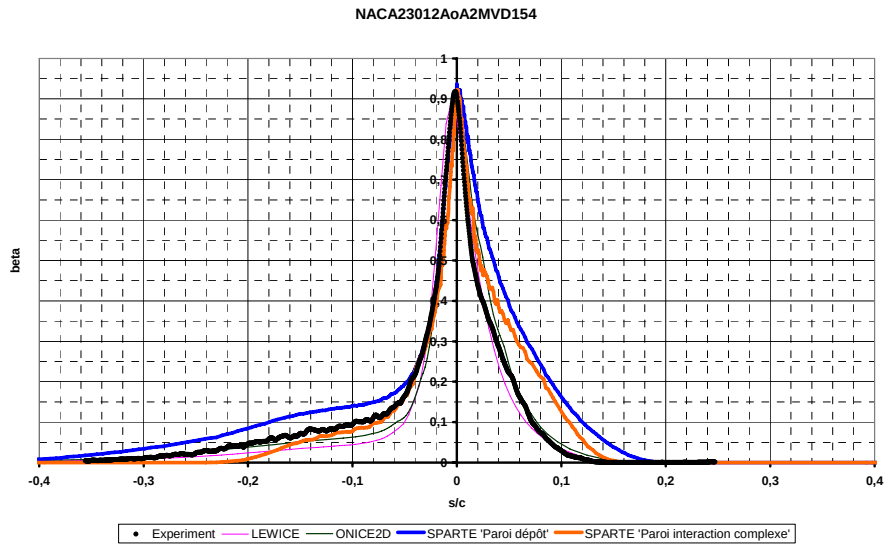


***Fig. 7: NACA23012 - Collection efficiency, MVD = 154 μm***

*Black line: experiment - Blue line: ONICE3D without SLD model - Orange line: ONICE3D with SLD model*

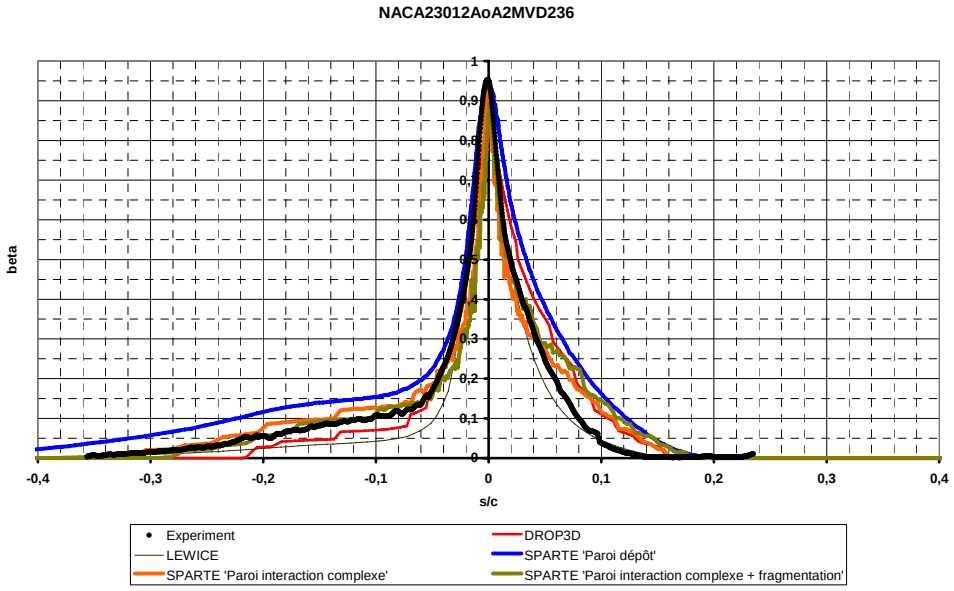


***Fig. 8: NACA23012 - Collection efficiency, MVD = 236 μm***

*Black line: experiment - Blue line: ONICE3D without SLD model*

*Orange line: ONICE3D with SLD model – Brown line: ONICE3D with SLD model + break-up model*

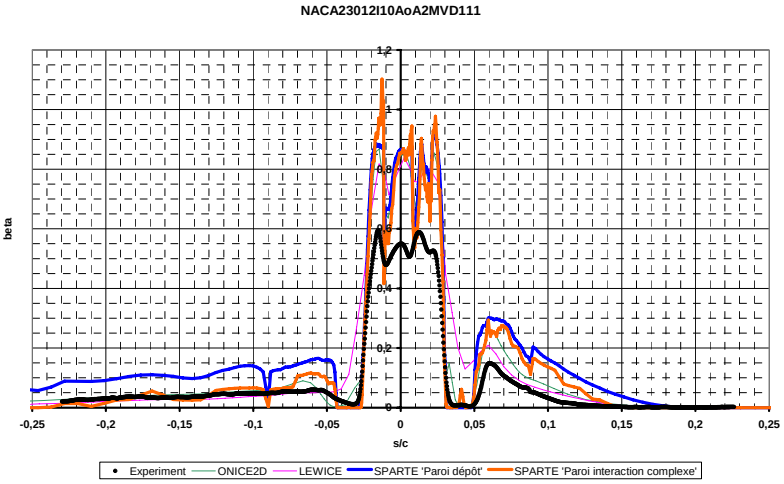


***Fig. 9: NACA23012 - Collection efficiency, Ice shape effect***

*Black line: experiment - Blue line: ONICE3D without SLD model - Orange line: ONICE3D with SLD model*

In Fig. 9, it is worth noticing that, in the case of the NACA airfoil with ice shape, all models tend to strongly overestimate the collection efficiency coefficient near the leading edge and on the suction side of the airfoil. Here, roughness effects could be suspected to play an important role but, even for that case, we have kept the same value for the mean wall roughness height ($h_R$ = 20 µm)

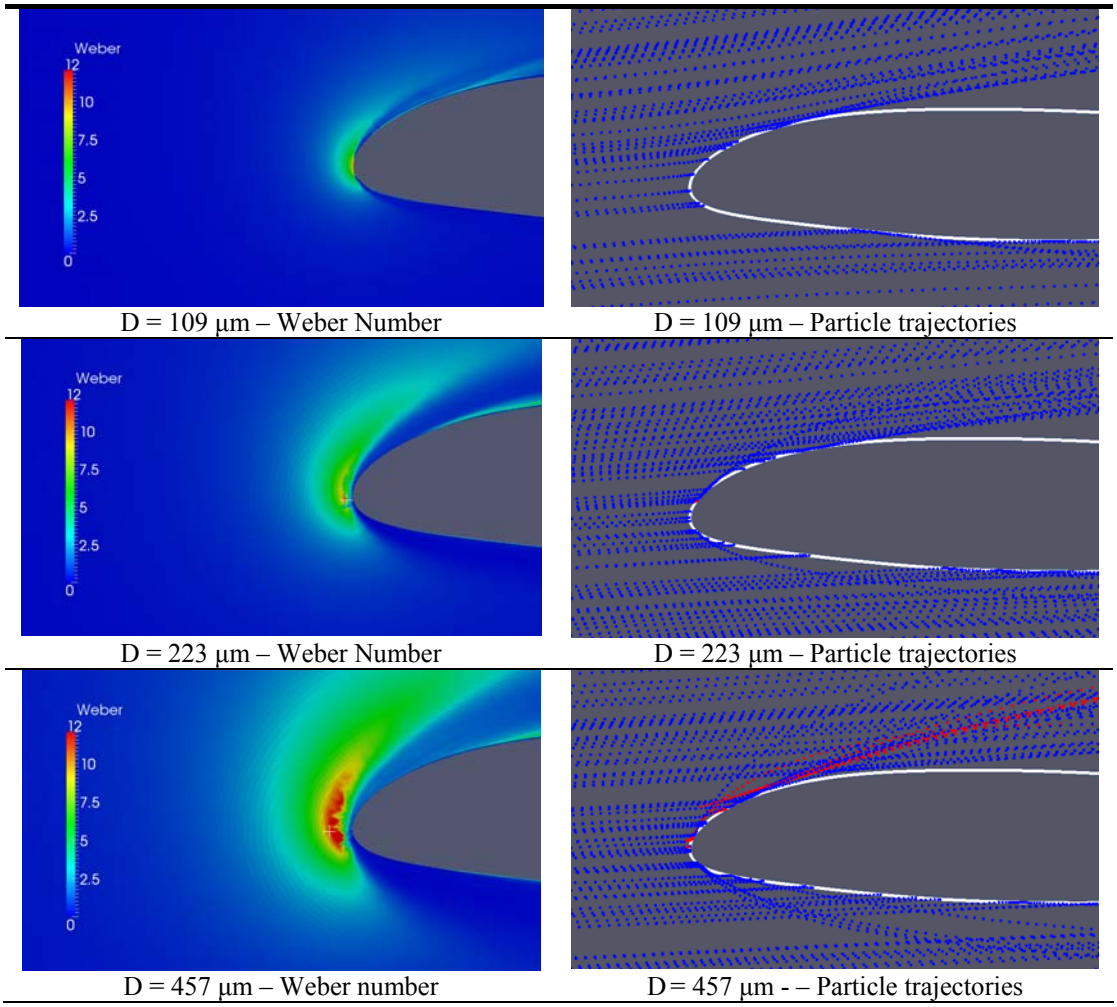


D = 109 µm – Weber Number | D = 109 µm – Particle trajectories

D = 223 µm – Weber Number | D = 223 µm – Particle trajectories

D = 457 µm – Weber number | D = 457 µm - – Particle trajectories

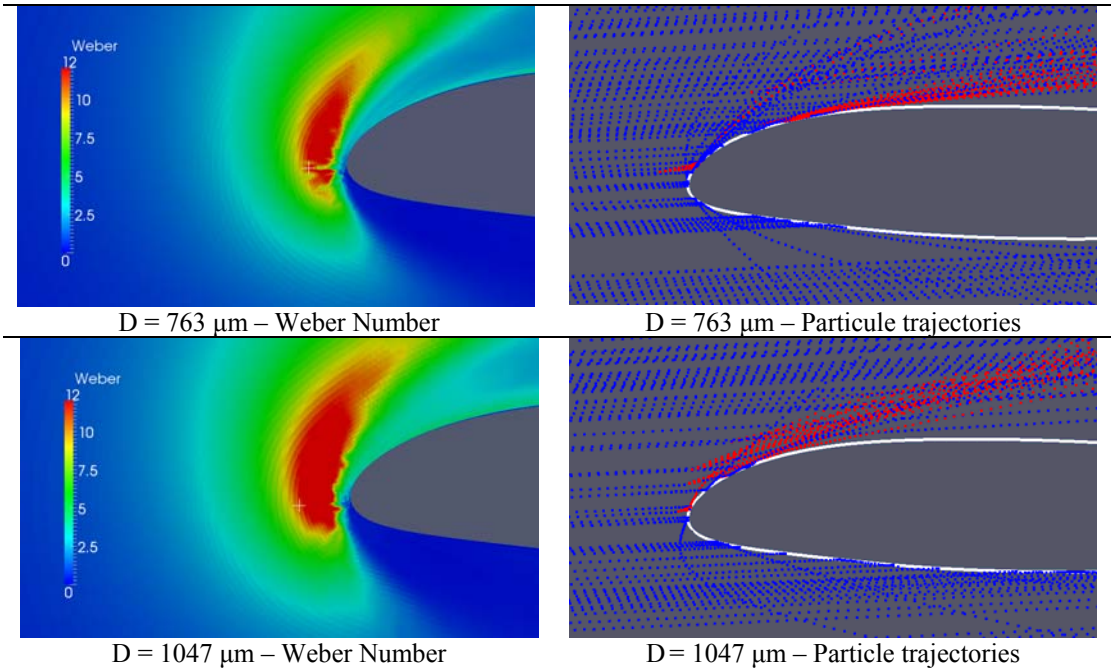


***Fig. 10:*** *NACA23012 - Influence of the secondary break-up process on droplet trajectories. Only a few randomly chosen trajectories have been plotted.*

## V. Conclusion

A SLD model is now available in the Lagrangian module of ONERA 3D icing suite. This model has been partially assessed using some tests from the NASA SLD experimental database. Its activation yields significantly improved collection efficiency predictions but discrepancies are still present, mainly on the suction side and near the stagnation point in case of an airfoil with ice shape. Results have also been compared to those of LEWICE and can be considered of comparable accuracy.

Looking to the future, the model has still to be improved and more accurately validated, especially regarding impact regime thresholds, roughness influence and film thickness effects. Moreover, the necessity of introducing an explicit influence of the incidence angle in the splashing mass loss model is not fully satisfactory from a theoretical point of view and alternative formulations are currently studied at ONERA.

Last but not least, the validation performed in this study was focused on collection efficiency experimental data. In the next step, we shall also consider SLD ice accretion experiments, including those performed in the frame of EXTICE European project (FP7) and perform the assessment of the whole 3D accretion chain.

**Acknowledgements.** The authors thank Fabien Dezitter from Airbus-France for helpful discussions and providing data for model assessment.

## VI. References

[1]Fabien Dezitter, "ONICE2D and DROP3D SLD Capability Assessment", *SAE International Conference on Aircraft and Engine Icing and Ground Deicing*, paper 38-0088, Chicago (USA), 2011.

[2]N.G. Garcia, P. Villedieu, J. Dewitte, G. Lavergne, "A new droplet-wall interaction model", *ICLASS06-167*.

[3]W.B. Wright, M.G. Potapczuck, "Semi-Empirical Modeling of SLD physics", *AIAA-2004-0412*.

[4]M.F. Trujillo, W., S. Mathews, C.F. Lee, J.E. Peters, "Modelling and experiments of impingement and atomisation of a liquid spray on a wall", I*nternational journal of engine research*, Vol. 1, No. 1, 2000, pp. 87-105.

[5]M. Papadakis, A. Rachman, S. C. Wong, H. Yeong, K. E. Hung, G. T. Vu, and C. S. Bidwell. "Water droplet impingement on simulated glaze, mixed and rime ice accretions". *Technical Report NASA/TM-2007-213961,NASA*, October 2007

[6a]A. Refloch et al, "CEDRE software", *Aerospace Lab n°2*, 2011

[6b]"CEDRE – Calcul d'Ecoulements (Diphasiques)(Réactifs) pour l'Energétique", URL : http://cedre.onera.fr [cited 31 May 2012].

[7]A. Muronne, Ph. Villedieu, "Numerical Modeling of Dispersed Two-Phase Flow", *Aerospace Lab n°2*, 2011.

[8a]LP. Hsiang, GM. Faeth, "Near-limit drop deformation and secondary breakup", *Int. J. of Mult. Flow*, Vol. 18, No. 5, 1992, pp. 635-652

[8b]LP. Hsiang, GM. Faeth, "Drop properties after secondary breakup", *Int. J. of Mult. Flow*, Vol. 19, No. 5, 1993, pp. 721-735

[9]AA. Amsden, JD. Ramshaw, PJ. O'Rourke, JK. Dukowicz, "KIVA: A computer program for two- and three-dimensional fluid flows with chemical reactions and fuel sprays", *Los Alamos National Lab* (USA), 1985.

[10]KL. Wert, "A rationally-based correlation of mean fragment size for drop secondary breakup, *Int. J. of Mult. Flow*, Vol. 21, No. 6, 1995, pp. 1063-1071

[11]R. Schmehl, H. Rosskamp, M. Willmann, S. Wittig, "CFD Analysis of Spray Propagation and Evaporation Including Wall Film Formation and Spray/Film Interactions", *Int. J. of Heat and Fluid Flow*, Vol. 20, No 5, 1999, pp. 520-529.

[12]C.H.R. Mundo, M. Sommerfeld, & C. Tropea, "Droplet-wall collisions: experimental studies of the deformation and break-up process", *Int. J. of Multiphase Flow*, Vol. 21, No. 2, 1995, pp. 151-173.

[13]J. Dewitte, P. Berthoumieu, G. Lavergne, "An Experimental Study of Droplet Hot Wall Interactions and a Survey of the Splashing Regime, 5th International Symposium on Multiphase Flow", *Heat Mass Transfer and Energy Conversion, ISMF 05 Xi'an, China*, 3-6 July 2005